U. Walzer, R. Hendel, and J. Baumgardner. Plateness of the oceanic lithosphere and the thermal evolution of the Earth's mantle. In W. E. Nagel, W. Jäger, and M. Resch, editors, High Perf. Comp. Sci. Engng. '05, pages 289-304. Berlin, 2006.

Plateness of the oceanic lithosphere and the thermal evolution of the Earth's mantle

Uwe Walzer[1], Roland Hendel[1], and John Baumgardner[2]

[1] Institut für Geowissenschaften, Friedrich-Schiller-Universität, Burgweg 11, 07749 Jena, Germany
[2] Dept. Earth Planet. Science, University of California, Berkeley, CA 94720, USA

Summary. Compared to [34], the model of the thermal evolution of the Earth's mantle is considerably improved. The temporal development of the radial viscosity profile due to cooling of the Earth could substantially be taken into account by numerical progress using a new variant of the temperature- and pressure-dependence of the shear viscosity of the mantle, namely Eq (5). The laterally averaged heat flow, the Urey number, the Rayleigh number and the volume-averaged temperature as a function of time come up to the expectations that stem from the parameterized evolution models. The mentioned evolution parameters of the present paper better approximate the observational data. Contrary to the parameterized curves, these quantities show temporal variations. This seems to be more realistic for geological reasons. Due to the activation enthalpy, the presented viscosity profile has a highly viscous transition layer (TL) with steep viscosity gradients at the phase boundaries. A low-viscosity zone is situated above and below the TL, each. The lithosphere moves piecewise en bloc. Thin cold sheet-like downwellings have an Earth-like distribution.

1 Introduction

The present dynamical model of the Earth's mantle *simultaneously* generates good self-consistent plateness of the oceanic lithosphere and a proper approximation of general thermal evolution parameters as a function of time. This second point of view is often treated by another kind of models. In these parameterized models, the creeping-velocity and the temperature fields are not computed in detail but taken into consideration in the energy balance only by a relation between Nusselt number, Nu, and Rayleigh number, Ra. According to Schubert et al. (1979, 1980), the energy conservation can be expressed in a simplified way:

$$M \cdot c \cdot \frac{\partial \overline{T}}{\partial t} = M \cdot H_0 \cdot e^{-\lambda t} - \frac{A \cdot k \cdot (\overline{T} - T_0)}{d} \cdot \left(\frac{Ra}{Ra_{cr}} \right)^{\beta} \qquad (1)$$

where M is the mass of the Earth's mantle, c is its specific heat, $\overline{T}$ is the

volume-averaged mantle temperature, t is the time, H_0 is the specific radiogenic heat production rate at the beginning of the evolution, λ is a generalized decay constant, k is the thermal conductivity, d is the thickness of the mantle, T_0 is the fixed surface temperature, Ra_{cr} is the critical Rayleigh number, A and β are constants. There are different planetary heat transport mechanisms since, due to the dependence of the viscosity on temperature and volatiles, different regimes develop near the surface: mobile regime, plate-tectonic regime and stagnant-lid regime. Separate *Nu-Ra* parameterizations for each mode have been derived by Solomatov (1995) and Reese et al. (1998, 1999). In the present paper, however, we solve the full set of the equations of mass, momentum and energy in a viscous compressible spherical shell with yield stress. For the special form of the equations see Chapter 3.2 by Walzer et al. (2003a). For the implementation of the yield stress see Walzer et al. (2004a). All equations have been simultaneously solved at 1351746 nodes of the mantle grid for each time step of the 4.49×10^9 years of the mantle evolution. So, the computed evolution starts at a time when the chemical differentiation of the Earth's core was certainly finished. Some runs were made with 10649730 nodes to check the convergence. The focus of this paper is to compare the temporal devel-

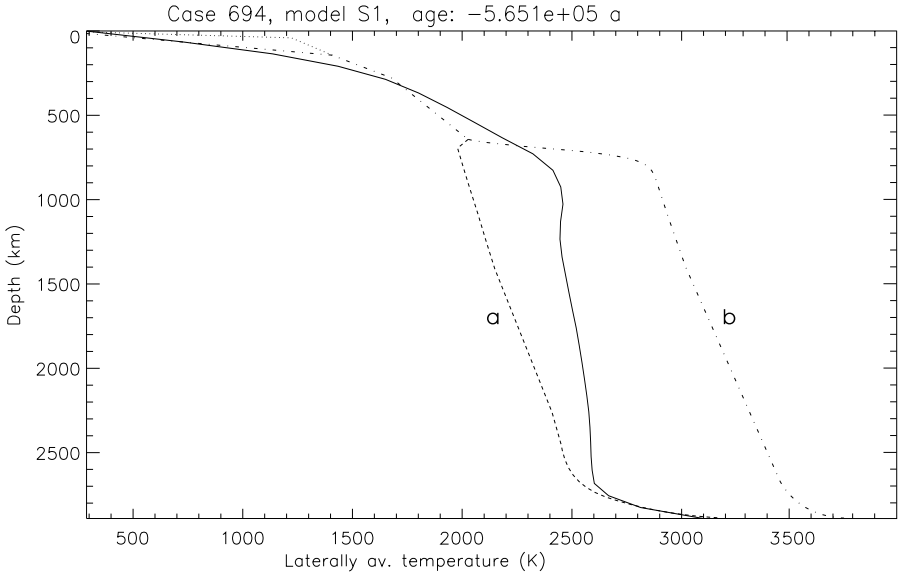

Fig. 1. The solid curve denotes the laterally averaged temperature of the geological present time for the reference run of this paper with $\sigma_y = 135\ MPa$. The CMB temperature, T_c, is spacially constant but variable in time according to the heat balance of the Earth's core. The range of possible mantle geotherms according to Schubert et al. (2001) is shown for comparison. Label *a* and *b* refer to geotherms of whole-mantle and partially layered convection, respectively. The dotted line represents the ridge geotherm.

opment of global thermal numbers with those of parameterized models, e.g. Schubert et al. (2001), and to show the general planform of the convection. So, the second main task of this paper is to show the self-consistent generation of oceanic lithospheric plates with Earth-like distribution of the subduction zones. Other authors made other numerical experiments with some kinds of constitutive equations to produce subducting plates, e.g. pseudoplastic yielding, strain weakening (Tackley, 2000a, 2000b), self-lubrication and viscoplastic yielding (Bercovici, 1998; Moresi and Solomatov, 1998; Richards et al., 2001). Trompert and Hansen (1998) used a strongly temperature-dependent viscosity with yield stress and found episodic plate-like motion with long time spans with a stagnant lid. Auth et al. (2003) used 2-D simulations with temperature- and damage-dependent viscosity. In dependence on the damage source term, they found four different convective regimes. The plate-like regime is characterized by focused low-viscosity bands, homogeneous surface velocities, and asymmetric subduction of the slab. Funiciello et al. (2003) used 2-D numerical experiments to investigate how rheology influences slab dynamics and slab-mantle interaction. Regenauer-Lieb and Yuen (2003) studied the slab mechanisms in connection with shear localization and mylonitic shear zones. Morra and Regenauer-Lieb (2004) presented an approach to solve the problem of a cold subducting slab into a hot fluid-like mantle. For this purpose,

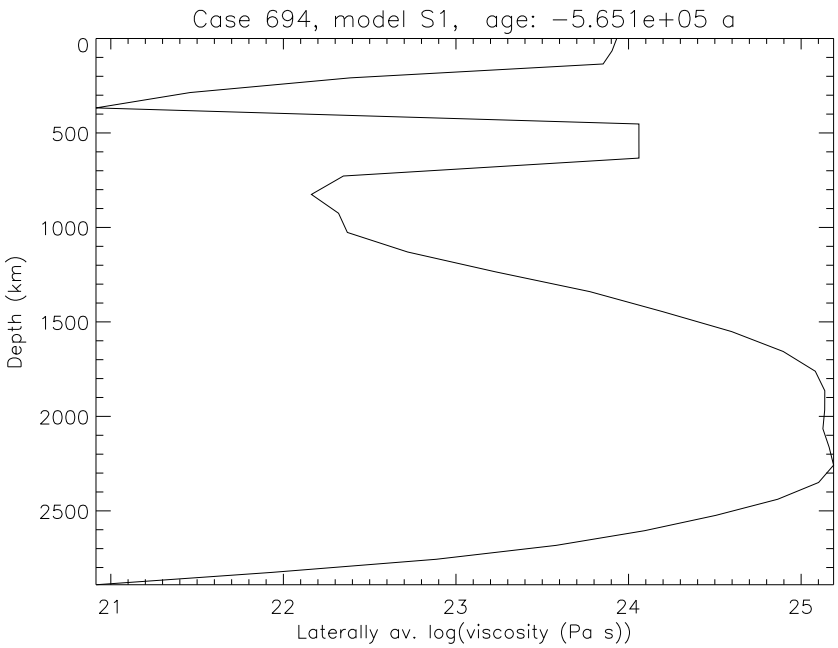

Fig. 2. The laterally averaged viscosity of the reference run for the geological present.

they join the Boundary Element Method and the Finite Element Method. It is evident that the latter three papers cannot be used in our code because of the demanded grid-point density. – In addition, the rheology of the subduction zones has been investigated in considerably more details. Karato et al. (2001) incorporated grain-size, stress, temperature and pressure dependence of the rheology. They studied diffusional creep, dislocation creep and the Peierls mechanism of the relevant minerals and found that the rheological structure of the slab varies laterally and with depth. For the deep slab, they found a weak, fine-grained spinel region wrapped up in a narrow but strong skin. Further details of the mineralogy of the subducting lithospheric slab are given by Weidner et al. (2001) and Bina et al. (2001). At present it is not possible to incorporate these findings in detail into our model because of lack of computing time.

Stein et al. (2004) explored the self-consistent formation of plates in a 3-D Cartesian box model. For temperature- and stress-dependent rheology, they

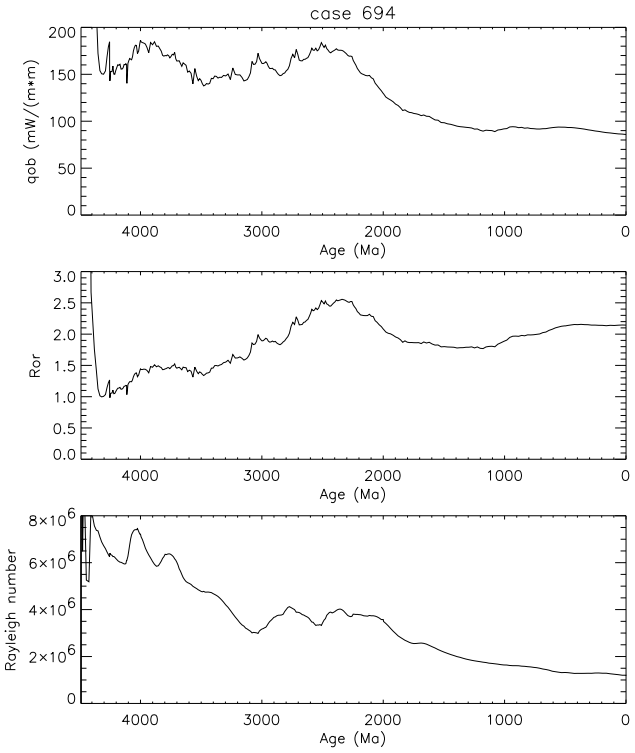

Fig. 3. The evolution of the laterally averaged surface heat flow, *qob*, of the *r*atio of the surface heat *o*utflow per unit time to mantle's *r*adiogenic heat production per unit time, *Ror*, and of the Rayleigh number, *Ra*.

obtained plates. But the plate motion only exists during short intervals followed by long time spans of an immobile lid. However, adding the pressure dependence of the viscosity and of the thermal expansitivity, they found a continuous plate motion and a low-viscosity zone. They varied the parameters and found that plate-like behavior is restricted to a narrow window of parameters.

2 The model

Walzer et al. (2003b, 2004a, 2004b) found the self-consistent formation of slabs and continuous plate motion in a 3-D spherical-shell model. We used a viscous model supplemented by a viscoplastic yield stress, σ_y, for the uppermost 285 km of the mantle. In this upper zone, an effective viscosity, η_{eff}, was implemented

$$\eta_{eff} = min\left[\eta(P,T), \frac{\sigma_y}{2\dot{\varepsilon}}\right] \tag{2}$$

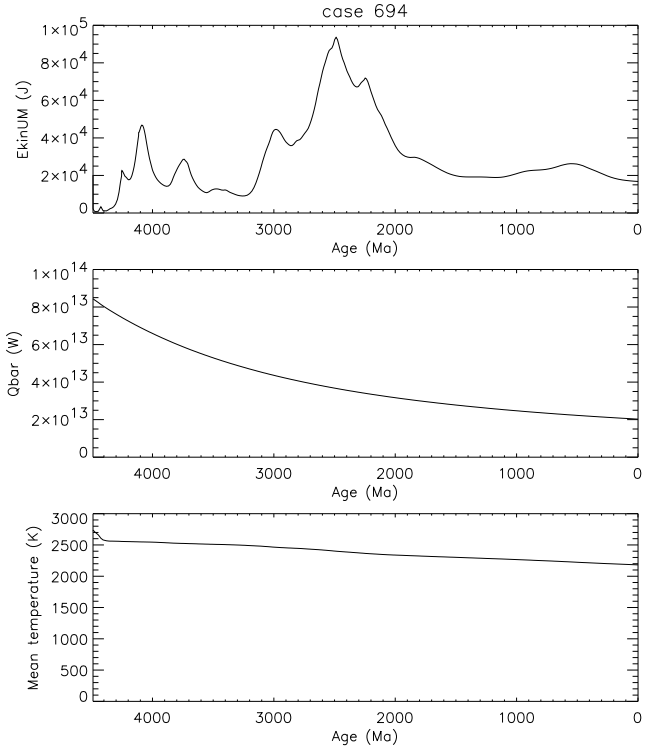

Fig. 4. The evolution of the kinetic energy of upper-mantle convection, $EkinUM$, the power of the internal heat generation of the mantle, $Qbar$, and the volume-averaged mean temperature of the mantle.

and used instead of the shear viscosity, η. The second invariant of the strain-rate tensor is denoted by $\dot{\varepsilon}$, P is the pressure, T is the temperature. In [33,34], the parameters have been varied and a central Rayleigh-number–yield-stress range with continuous plate-like motion was found. However, we use an infinite Prandtl number fluid in a compressible spherical shell. This shell is heated from within by a homogeneous distribution of the major heat-producing elements with the abundances of the primordial mantle according to McCulloch and Benett (1994). Therefore, the heating power decreases as a function of time. We [32] parameterized the pressure, P, density, ρ, bulk modulus, K, and dK/dP using a Birch-Murnaghan equation of state and PREM (Dziewonski and Anderson, 1981). So, using the Vashchenko-Zubarev (1963) gamma, we are able to directly derive the Grüneisen parameter, γ, from seismic observations. Introducing an experimental thermal expansivity, α, that decreases with increasing pressure, we [32] obtained also the specific heat at constant pressure, c_p, and the specific heat at constant volume, c_v, as a function of depth. We derived a viscosity profile with considerable viscosity gradients at the upper and lower boundaries of the transition layer. We could use it only in [33, 34, 35] and in the present paper because of improvements of the numerics. In [32] only an approximation was applied. The mentioned steep viscosity gradients are caused by jumps of the activation volume, V^*, and of the activation energy, E^*, at the mineral phase boundaries. A second way to derive the radial dependence of the viscosity is to compute the melting temperature, T_m, by Gilvarry's (1956) formulation of Lindemann's law and by

$$\eta = \eta_0 \cdot \exp\left(\frac{k_2 T_m}{T}\right) \tag{3}$$

The direct use of Eq (3) generates big numerical difficulties because of steep viscosity gradients. Therefore, the following approximation of Eq (3) was introduced in [34]:

$$\eta(r,\theta,\phi,t) = 10^{r_n} \cdot \eta_3(r) \cdot \exp\left[c_t \cdot T_m(r) \cdot \left(\frac{1}{T(r,\theta,\phi,t)} - \frac{1}{T_{av}(r,t)}\right)\right] \tag{4}$$

where T_{av} is the laterally averaged temperature, r the radius, θ the colatitude, ϕ the longitude, t the time, c_t a constant and r_n the viscosity-level parameter. The quantity r_n is zero for Eq (3). It serves only for the shift of he viscosity profile during the variation of the parameters. Up to now, we had ignored the temporal dependence of η_3. This fact misrepresented the thermal evolution behavior of the model whereas the general circulation, the generation and distribution of the oceanic lithospheric plates and of the subduction zones showed a good Earth-like behavior. Due to improvements of the code, we are able to replace Eq (4) by

$$\eta = 10^{r_n} \cdot \frac{exp(c\ \overline{T_m/T_{av}})}{exp(c\ \overline{T_m/T_{st}})} \cdot \eta_3(r) \cdot exp\left[c_t \cdot T_m \left(\frac{1}{T} - \frac{1}{T_{av}}\right)\right] \tag{5}$$

in this paper. The bar denotes the radial average, T_{st} the initial temperature profile. By Eq (5), the viscosity profile has rising values with the cooling of the Earth. So, the real thermal evolution is better reflected by the present model than in [34]: The increasing average viscosity of the cooling mantle is essentially taken into account without loss of plateness and other successful features of the previous model. For $MgSiO_3$ perovskite we should insert $c = 14$, for MgO wüstite $c = 10$ according to Yamazaki and Karato (2001). So, the lower-mantle c should be between 10 and 14. However, for numerical reasons we can use only $c = 7$. The lateral variability of viscosity is described only by the fourth factor of the right-hand side of Eq (5). For the present reference run, we take $c_t = 1, \quad r_n = -0.6$ and $\sigma_y = 135\ MPa$.

3 Results

We anticipate that the features of the presented solution apply for a wider range of the values of temporally averaged Rayleigh number and yield stress. Fig. 1 presents the laterally averaged temperature profile of the geological

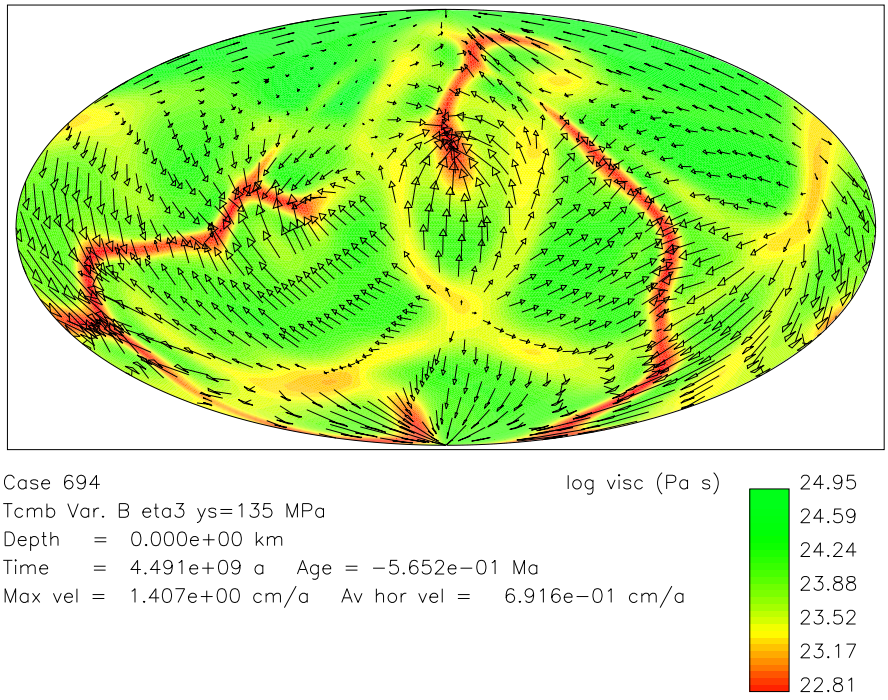

Fig. 5. The surface distribution of log viscosity for a yield stress, σ_y, of 135 MPa. The creeping velocities (arrows) show a good plate-tectonic behavior. Elongated high strain-rate zones have reduced viscosity due to plastic yielding.

present. As expected, $T_{av}(r)$ is nearer to the parameterized profile, a, for whole-mantle convection since this kind of convection is hindered by the high-viscosity transition layer of the model but not prevented. The present T_{av} curve lies nearer to the curve a than the corresponding curves of Fig. 3 of [34], mainly in the lower region of the lower mantle since the second factor of Eq (5) allows a stronger, and therefore more realistic, cooling of the mantle. The sharp bend of the T_{av} curve of Fig. 1 reminds one of the scheme of the plate-tectonics isotherm in Fig. 2.1 of Breuer (2003), although the cause of the sharp bend there stems from the thermal lithosphere.

Fig. 2 shows the characteristic present-day viscosity profile of the present paper. A highly viscous lithosphere is on top as expected. Below of it, is an asthenosphere. The low-viscosity region of it corresponds to the Haskell (1935) value. New features of this profile are a high-viscosity transition layer with steep viscosity gradients at the boundaries. The latter fact is in contrast with [32]. Further new features are a second low-viscosity layer below the 660-km phase boundary, considerably high viscosity in the thick middle part of the lower mantle with good opportunities to preserve primordial chemical inhomogeneities in that region and a strong decrease of the viscosity down to the D" layer. We found similar features in our earlier papers but the numerical values of the extreme viscosity values vary. Cf. Table 1.

Table 1. The extreme values of different viscosity profiles of the reference runs

Paper	[32]	[34]	[35], first part	[35], second part	this paper
Figure	1	4	6, fourth panel	15	2
$\sigma_y(MPa)$	∞	135	∞	135	135
Dimensions	3-D	3-D	2-D	3-D	3-D
max $\log \eta_{av}(Pa\ s)$ of lithosphere	22.68	23.71	25.2	23.71	23.92
min $\log \eta_{av}(Pa\ s)$ of asthenosphere	21.0	20.56	20.1	20.56	20.92
max $\log \eta_{av}(Pa\ s)$ of TL	23.7	23.7	25.5	23.7	24.5
max $\log \eta_{av}(Pa\ s)$ of LM	24.6	24.9	24.7	24.9	25.2

Figs. 3 and 4 present essential improvements in the model of thermal evolution in comparison with earlier papers. In [32], i.e. the model without yield stress, σ_y, and without plates, the laterally averaged heat flow, *qob*, decreases as a function of time to 73.98 mW/m^2 for the reference run, to values somewhat below the observed values also for the other runs. In [34], i.e. a model with σ_y and with plates, *qob* decreases only since an age of $\tau \approx 2400\ Ma$ only very slightly down to 104.4 mW/m^2 that lies above the observed value. However, the first panel of Fig. 3 of this paper shows that, starting with very high values, *qob* strongly decreases with some temporal variations in

the Archean and the Proterozoic down to 85.86 mW/m^2 now. The observed present-day *qob* is 82 mW/m^2. This behavior is well matched to parameterized models, e.g. by McGovern and Schubert (1989). According to the design, no temporal variations are possible in parameterized models. But geology teaches that variations are realistic.

The reciprocal value, *Ror*, of the Urey number of [32] increases during the first half of the Earth's evolution and is nearly constant in the second half. [34] is characterized by continuous rise of *Ror* during the whole Earth's history. According to parameterized models (see McGovern and Schubert (1989) and Schubert et al.(2001), p. 603), a strong decrease of *Ror* is to be expected for the earliest history and a gradual rise of *Ror* in the big rest of the evolution. The second panel of Fig. 3 shows that our *Ror* sharply diminishes at the very beginning, but than *Ror* gradually increases with some temporal variations. Stacey and Stacey (1999) derived an averaged value of 1.85 for *Ror* of the last 2000 Ma. We arrive at about 2.00, that is somewhat too high. In summary, $Ror(\tau)$ of this paper seems to be more realistic than that of [32] and [34].

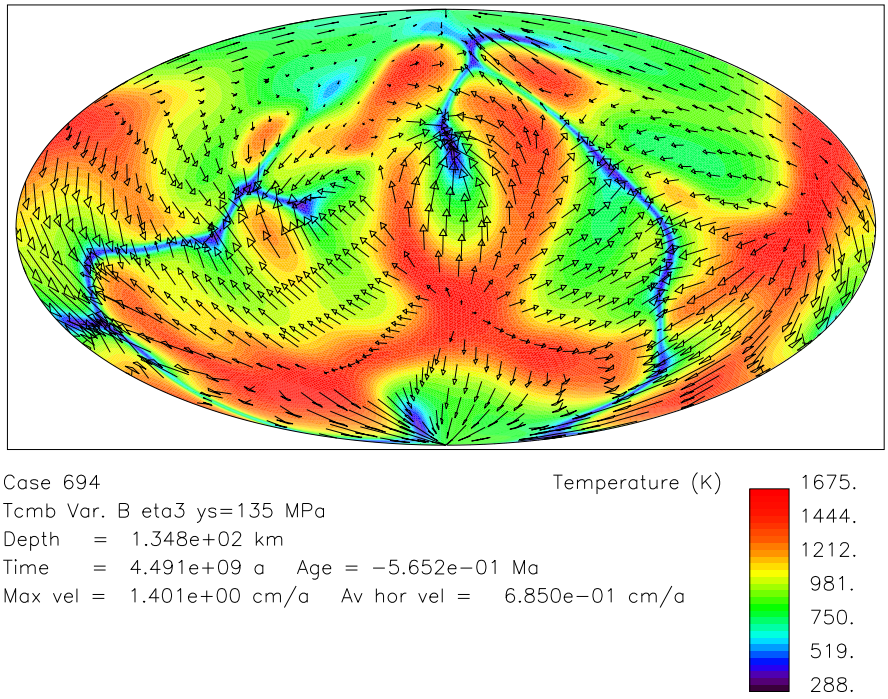

Fig. 6. Temperature distribution (colors) and creeping velocities (arrows) of our reference run for the geological present, for 134.8 km depth and $\sigma_y = 135\ MPa$. The narrow blue downwelling zones can be pursued in the deeper equal-area projections of temperature distribution. The "slabs" are rather narrow in comparison with the broad upwelling zones.

The Rayleigh number, Ra, decreases also in [32] and [34] but essentially less than demanded by parameterized models. The first panel of Fig. 3 presents now an considerably stronger decrease of Ra. The real magnitude of Ra cannot be reached for numerical reasons as in dynamical calculations of other workers, too. So the present model reflects rather well not only plateness and subduction but also the thermal evolution. For numerical reasons, the model is stiffer than the real Earth.

The kinetic energy of the upper mantle, $EkinUM$, can be considered as a measure of the power transmission to the oceanic lithospheric plates. The first panel of Fig. 4 presents a pronounced maximum at the turn from Archaic to Proterozoic, at $\tau = 2500\ Ma$. The radiogenic heating from within of the mantle non-linearly decreases as a function of time. That is depicted in the second panel of Fig. 4. – Although the volume-averaged temperature, T_{mean}, grows down as a function of time in [32], it is somewhat to low. In [34], however, T_{mean} is higher but at first it rises slowly until an age of $\tau = 3000\ Ma$ is reached. From this time, it decreases until the present time but much less steeply than expected by parameterized models. The third panel of Fig. 4, however, shows that, at first, T_{mean} decreases stronger, then moderately grows down until the present time. T_{mean} descends by 400 K during the

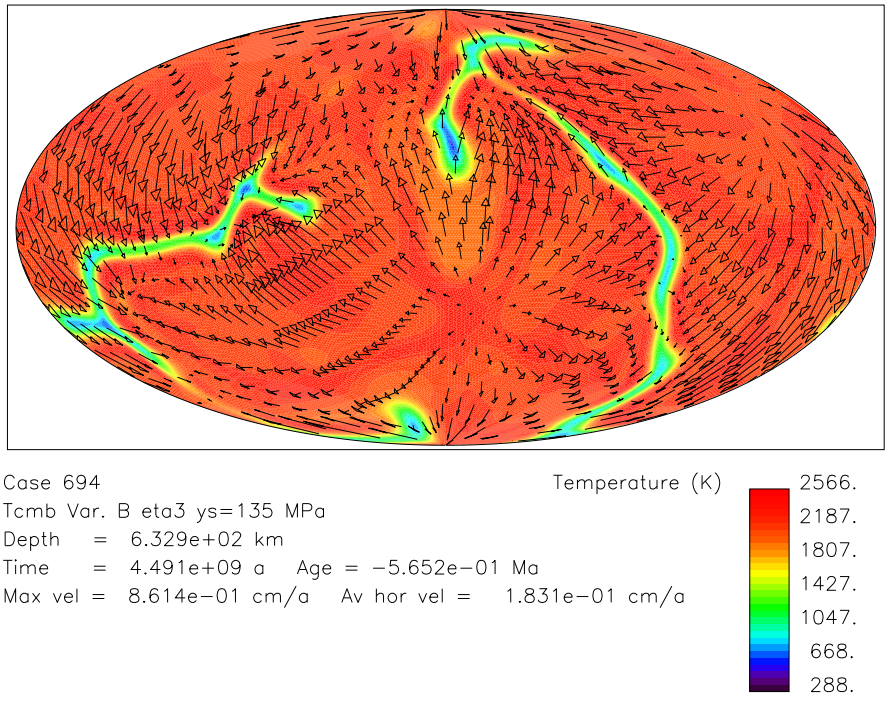

Fig. 7. Temperature distribution and creeping velocities for 632.9 km depth.

last 4000 Ma. These values correspond to the results of komatiite research. Parameterized models give similar results.

Fig. 5 reveals that pieces of the surface move with spatially constant angular velocity. So, they flow plate-like. Only relatively small boundary areas don't fit in this simplified picture. But also on the real Earth, some plate boundaries are somewhat extended (Gordon 2000). So, Fig. 5 seems to be rather realistic apart from the missing continents. In our next paper, we want to include the evolution of continents by chemical differentiation. Already [33] and [34], we found plate-like solutions near the Earth's surface. In [32], however, the upwelling currents show star-shaped, divergent flow lines at the surface. That behavior is well-known from purely viscous models.

Fig. 6 depicts an equal-area plot of the temperature distribution (colors) and the creeping velocities (arrows) for the geological present in 134.8 km depth. The distribution of the arrows reminds one of the plate-tectonic picture of the surface, yet. The downwelling areas are very sharp lines compared with the broad upflow areas. The distribution of this slab-like features is Earth-like and not reticular as in [32], yet. But also [32] was characterized by a very small thickness of the cold sheet-like downwellings. In [34] and Fig. 6, however, we have an Earth-like distribution of thin cold sheet-like downwellings.

Fig. 7 shows the temperature and velocity distribution in 632.9 km depth, in the transition layer, yet. As in all upper spherical surfaces, the solid creeps toward the slab-like features. Fig. 8 is the first shown picture of this kind that is situated in the lower mantle: The cold downwellings are somewhat more diffusely distributed. The material begins to flow divergently away from the cold zone. Fig. 9 demonstrates that the mentioned tendencies of Fig. 8 are stronger in 1864 km depth. Although the cold zone is at the expected place, yet, its distribution is rather broad as it is observed in the continuations of the slabs in the real lower mantle.

4 Numerical and computational aspects

We solved the system of differential equations of convection in a compressional spherical shell in the special form of [32] and [34] using a three-dimensional finite-element discretization, a fast multigrid solver and the second-order Runge-Kutta procedure. The mesh is generated by projection of a regular icosahedron onto a sphere to divide the spherical surface into 20 spherical triangles or 10 spherical diamonds. A dyadic mesh refinement procedure connects the mid-points of each side of a triangle with a great circle such that each triangle is subdivided into four smaller triangles. Successive grid refinements produce an almost uniform triangular discretization of the spherical surface of the desired resolution. Corresponding mesh points of spherical surfaces at different depths are connected by radial lines. The radial distribution of the different spherical-surface triangular networks is so that the volumes of the cells are nearly equal. More details are given by Baumgardner (1983, 1985),

Bunge et al. (1997) and Yang (1997). For the most runs, we employed a mesh with 1351746 nodes. Some runs were made with 10649730 nodes to check the convergence of the lower resolution runs. The result is that the laterally averaged heat flow, the ratio of heat outflow to radiogenic heat production, the Rayleigh number, and the Nusselt number as functions of time show hardly discernable differences. The calculations were performed on 32 processors of a Cray Strider Opteron cluster. A scalability test showed a scaling degree of nearly 90%. The code was benchmarked for constant viscosity convection by Bunge et al. (1997) with numerical results of Glatzmaier (1988) for Nusselt numbers, peak temperatures, and peak velocities. A good agreement was found. – The conclusions are condensed in the summary.

Acknowledgements

We want to thank Woo-Sun Yang for his kind help and interesting discussions. Two of us (U.W. and R.H.) gratefully acknowledge the hospitality of Charles Keller, LANL, Los Alamos, NM. This research was supported by the Volkswagenstiftung through the grant I75474, by the Höchstleistungsrechenzentrum der Universität Stuttgart (HLRS), and by the John von Neumann Institute

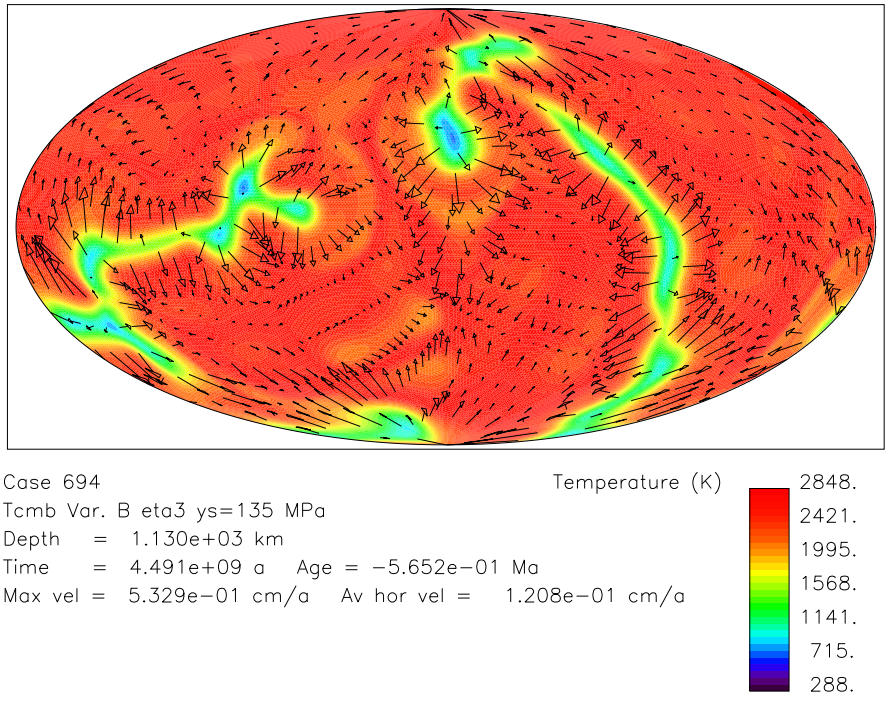

Fig. 8. Temperature distribution and creeping velocities for 1130 km depth.

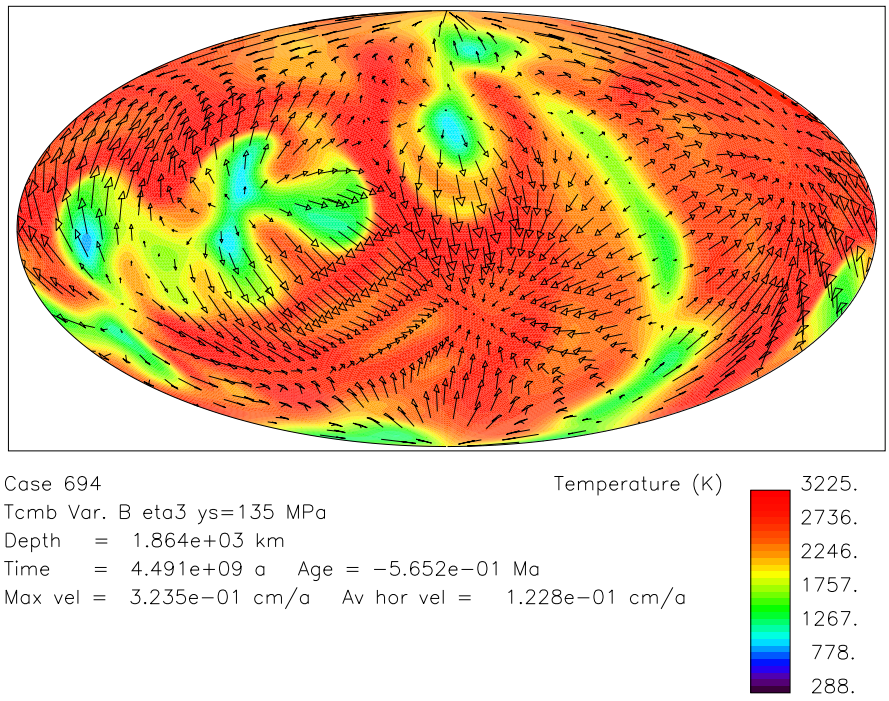

Fig. 9. Temperature distribution and creeping velocities for 1864 km depth.

of Computing, Forschungszentrum Jülich, through the supply of computing time.

References

[1] Auth, C., Bercovici, D., Christensen, U.R., 2003. Two-dimensional convection with a self-lubricating, simple-damage rheology. Geophys. J. Int. 154, 783-797.

[2] Baumgardner, J.R., 1983. A three-dimensional finite element model for mantle convection. Thesis, Univ. of California, Los Angeles.

[3] Baumgardner, J.R., 1985. Three-dimensional treatment of convective flow in the Earth's mantle. J. Stat. Phys. 39 (5-6), 501-511.

[4] Bercovici, D., 1998. Generation of plate tectonics from lithosphere-mantle flow and void-volatile self-lubrication. Earth Planet. Sci. Lett. 154, 139-151.

[5] Bina, C.R., Stein, S., Marton, F.C., Van Ark, E.M., 2001. Implications of slab mineralogy for subduction dynamics. Phys. Earth Planet. Int. 127, 51-66.

[6] Breuer, D., 2003. Thermal evolution, crustal growth, and magnetic field history of Mars. Habilitationsschrift. Univ. Münster, 176pp.

[7] Bunge, H.-P., Richards, M.A., Baumgardner, J.R., 1997. A sensitivity study of three-dimensional spherical mantle convection at 10^8 Rayleigh number: effects of depth-dependent viscosity, heating mode, and an endothermic phase change. J. Geophys. Res. 102, 11991-12007.

[8] Dziewonski, A.M., Anderson, D.L., 1981. Preliminary reference Earth model. Phys. Earth Planet. Inter. 25, 297-356.

[9] Funiciello, F., Morra, G., Regenauer-Lieb, K., Giardini, D., 2003. Dynamics of retreating slabs: 1. Insights from two-dimensional numerical experiments. J. Geophys. Res. 108, no. B4, 2206, doi: 10.1029/2001JB000898

[10] Gilvarry, J.J. 1956. The Lindemann and Grüneisen laws. Phys. Rev. 102, 307-316.

[11] Glatzmaier, G.A., 1988. Numerical simulations of mantle convection: Time-dependent, three-dimensional, compressible, spherical shell. Geophys. Astrophys. Fluid Dyn. 43, 223-264.

[12] Gordon, R.G., 2000. Diffuse oceanic plate boundaries: Strain rates, vertically averaged rheology, and comparisons with narrow plate boundaries and stable plate interiors. In: Richards, M.A., Gordon, R.G., van der Hilst, R.D.(Eds.), The History and Dynamics of Global Plate Motions. Amer. Geophys. Union, Washington, DC, pp. 143-159.

[13] Haskell, N.A., 1935. The motion of a fluid under a surface load. 1. Physics 6, 265-269.

[14] Karato, S.-I., Riedel, M.R., Yuen, D.A., 2001. Rheological structure and deformation of subducted slabs in the mantle transition zone: implications for mantle circulation and deep earthquakes. Phys. Earth Planet. Inter. 127, 83-108.

[15] McCulloch, M.T., Bennett, V.C., 1994. Progressive growth of the Earth's continental crust and depleted mantle: geochemical constraints. Geochim. Cosmochim. Acta 58, 4717-4738.

[16] McGovern, P.J., Schubert, G., 1989. Thermal evolution of the Earth: Effects of volatile exchange between atmosphere and interior. Earth Planet. Sci. Lett. 96, 27-37.

[17] Moresi, L.N., Solomatov, V.S., 1998. Mantle convection with a brittle lithosphere: thoughts on the global tectonic styles of the Earth and Venus. Geophys. J. Int. 133, 669-682.

[18] Morra, G., Regenauer-Lieb, K., 2004. A coupled solid-fluid method for modeling subduction. Philosophical Magazine, London, submitted.

[19] Regenauer-Lieb, K., Yuen, D.A., 2003. Modeling shear-zones in geological and planetary science: solid- and fluid-thermal-mechanical approaches. Earth Science Reviews, submitted.

[20a] Reese, C.C., Solomatov, V.S., Moresi, L.-N., 1998. Heat transport efficiency for stagnant lid convection with dislocation viscosity: Application to Mars and Venus. J. Geophys. Res. 103, 13643-13657.

[20b] Reese, C.C., Solomatov, V.S., Moresi, L.-N., 1999. Non-Newtonian stagnant lid convection and magmatic resurfacing of Venus. Icarus 139, 67-80.

[21] Richards, M.A., Yang, W.-S., Baumgardner, J.R., Bunge, H.-P., 2001. Role of a low-viscosity zone in stabilizing plate tectonics: Implications for comparative terrestrial planetology. Geochem., Geophys., Geosystems vol. 2, paper no. 2000GC000115.

[22] Schubert, G., Cassen, P., Young, R.E., 1979. Subsolidus convective cooling histories of terrestrial planets. Icarus 38, 192-211.

[23] Schubert, G., Stevenson,D., Cassen, P., 1980. Whole planet cooling and the radiogenic heat source contents of the Earth and Moon. J. Geophys. Res. 85, 2511-2518.

[24] Schubert, G., Turcotte, D.L., Olson, P., 2001. Mantle Convection in the Earth and Planets. Cambridge Univ. Press, Cambridge etc, 940 pp.

[25] Solomatov, V.S., 1995. Scaling of temperature-dependent and stress-dependent viscosity convection. Phys. Fluids 7, 266-274.

[26] Stacey, F.D., Stacey, C.H.B., 1999. Gravitational energy of core evolution: implications for thermal history and geodynamo power. Phys. Earth Planet. Inter. 110, 83-93.

[27] Stein, C., Schmalzl, J., Hansen, U., 2004. The effect of rheological parameters on plate behaviour in a self-consistent model of mantle convection. Phys. Earth Planet. Inter. 142, 225-255.

[28] Tackley, P.J., 2000a. Self-consistent generation of tectonic plates in time-dependent, three-dimensional mantle convection simulations. 1. Pseudoplastic yielding. Geochem. Geophys. Geosyst., 1, Paper no. 2000GC000036

[29] Tackley, P.J., 2000b. Self-consistent generation of tectonic plates in time-dependent, three-dimensional mantle convection simulations. 2. Strain weakening and asthenosphere. Geochem. Geophys. Geosyst., 1, Paper no. 2000GC000043

[30] Trompert, R.A., Hansen, U., 1998. Mantle convection simulations with rheologies that generate plate-like behavior. Nature 395, 686-689.

[31] Vashchenko, V.Ya., Zubarev, V.N., 1963. Concerning the Grüneisen constant. Soviet Phys. Solid State 5, 653-655.

[32] Walzer, U., Hendel, R., Baumgardner, J., 2003a. Viscosity stratification and a 3-D compressible spherical shell model of mantle evolution. In: Krause,E., Jäger,W., Resch,M. (Eds.), High Performance Computing in Science and Engineering '03. Springer-Verlag, Berlin Heidelberg New York. pp.27-67. ISBN 3-540-40850-9.

[33] Walzer, U., Hendel, R., Baumgardner, J., 2003b. Generation of plate-tectonic behavior and a new viscosity profile of the Earth's mantle. In Wolf,D.,Münster,G.,Kremer,M. (Eds.), NIC Symposium 2004. NIC Series 20, pp. 419-428. ISBN 3-00-012372-5.

[34] Walzer, U., Hendel, R., Baumgardner, J., 2004a. The effects of a variation of the radial viscosity profile on mantle evolution. Tectonophysics, 384, 55-90.

[35] Walzer, U., Hendel, R., Baumgardner, J., 2004b. Toward a thermochemical model of the evolution of the Earth's mantle. In: Krause,E.,Jäger,W.,Resch,M. (Eds.), High Performance Computing in Science and Engineering '04. Springer-Verlag, Berlin Heidelberg New York. pp 395-454. ISBN 3-540-22943-4

[36] Weidner, D.J., Chen, J. Xu,Y., Wu, Y., Vaughan, M.T., Li, L., 2001. Subduction zone rheology. Phys. Earth Planet. Inter. 127, 67-81.

[37] Yamazaki, D., Karato, S.-I., 2001. Some mineral physics constraints on the rheology and geothermal structure of the Earth's lower mantle. American Mineralogist 86, 385-391.

[38] Yang, W.-S., 1997. Variable viscosity thermal convection at infinite Prandtl number in a thick spherical shell. Thesis, Univ. of Illinois, Urbana-Champaign.